AFRL-RX-WP-TP-2010-4158

THE ACTIVATED STATE FOR CROSS-SLIP AT SCREW DISLOCATION INTERSECTIONS IN FACE-CENTERED CUBIC NICKEL (PREPRINT)

Satish I. Rao

UES, Inc.

Dennis M. Dimiduk, Michael D. Uchic, and Christopher Woodward

Metals Branch
Metals, Ceramics & NDE Division

Jaafar A. El-Awady

Universal Technology Corporation

APRIL 2010

AIR FORCE RESEARCH LABORATORY
MATERIALS AND MANUFACTURING DIRECTORATE
WRIGHT-PATTERSON AIR FORCE BASE, OH 45433-7750
AIR FORCE MATERIEL COMMAND
UNITED STATES AIR FORCE

REPORT DOCUMENTATION PAGE

Form Approved
OMB No. 0704-0188

1. REPORT DATE *(DD-MM-YY)*	2. REPORT TYPE	3. DATES COVERED *(From - To)*
April 2010	Journal Article Preprint	01 April 2010 – 01 April 2010

4. TITLE AND SUBTITLE
THE ACTIVATED STATE FOR CROSS-SLIP AT SCREW DISLOCATION INTERSECTIONS IN FACE-CENTERED CUBIC NICKEL (PREPRINT)

5a. CONTRACT NUMBER
FA8650-04-D-5235

5b. GRANT NUMBER

5c. PROGRAM ELEMENT NUMBER
62102F

6. AUTHOR(S)
Satish I. Rao (UES, Inc.)
Dennis M. Dimiduk, Michael D. Uchic, and Christopher Woodward (AFRL/RXLM)
Jaafar A. El-Awady (Universal Technology Corporation)

5d. PROJECT NUMBER
2511

5e. TASK NUMBER
00

5f. WORK UNIT NUMBER
25110002

7. PERFORMING ORGANIZATION NAME(S) AND ADDRESS(ES)

UES, Inc.
4401 Dayton-Xenia Road
Dayton, OH 45432-1894

Metals Branch (AFRL/RXLM)
Metals, Ceramics & NDE Division
Materials and Manufacturing Directorate
Wright-Patterson Air Force Base, OH 45433-7750
Air Force Materiel Command, United States Air Force

Universal Technology Corporation
1270 North Fairfield Road
Dayton, OH 45432-2600

8. PERFORMING ORGANIZATION REPORT NUMBER

9. SPONSORING/MONITORING AGENCY NAME(S) AND ADDRESS(ES)
Air Force Research Laboratory
Materials and Manufacturing Directorate
Wright-Patterson Air Force Base, OH 45433-7750
Air Force Materiel Command
United States Air Force

10. SPONSORING/MONITORING AGENCY ACRONYM(S)
AFRL/RXLMD

11. SPONSORING/MONITORING AGENCY REPORT NUMBER(S)
AFRL-RX-WP-TP-2010-4158

12. DISTRIBUTION/AVAILABILITY STATEMENT
Approved for public release; distribution unlimited.

13. SUPPLEMENTARY NOTES
Journal article submitted to *Acta Materialia*. PAO Case Number: 88ABW-2010-0511; Clearance Date: 08 Feb 2010. Paper contains color.

14. ABSTRACT
We extend our recent work where a screw dislocation in FCC Ni was found to spontaneously attain a low-energy partially cross-slipped configuration upon intersecting a forest dislocation. Using atomistic (molecular statics) simulations with embedded atom potentials, we evaluate the activation barrier for a dislocation to transform from fully residing on the glide plane to fully residing on the cross-slip plane intersecting a forest dislocation. The activation energies were obtained by determining equilibrium configurations (energies) when variable pure tensile or compressive stresses are applied along the direction on the partially cross-slipped state. We show that the activation energy is a factor of 3 - 6 lower than that for cross slip in isolation via the Escaig process. Further, the activation barrier for cross-slip at these intersections is shown to be linearly proportional to (d/b)ln(d/b), as in the Escaig process, where 'd' is the Shockley partial dislocation spacing and 'b' is the Burgers vector of the screw dislocation. These results suggest that cross-slip should be preferentially observed at selected screw dislocation intersections in FCC materials.

15. SUBJECT TERMS
Cross-slip; Activation analysis, Atomistic simulations; Nickel; Escaig stresses

16. SECURITY CLASSIFICATION OF:			17. LIMITATION OF ABSTRACT:	18. NUMBER OF PAGES	19a. NAME OF RESPONSIBLE PERSON (Monitor)
a. REPORT	b. ABSTRACT	c. THIS PAGE			Christopher F. Woodward
Unclassified	Unclassified	Unclassified	SAR	42	19b. TELEPHONE NUMBER *(Include Area Code)* N/A

Standard Form 298 (Rev. 8-98)
Prescribed by ANSI Std. Z39-18

The Activated State for Cross-Slip at Screw Dislocation Intersections in Face-Centered Cubic Nickel

S.I. Rao*, D.M. Dimiduk, J.A. El-Awady#, T.A. Parthasarathy*, M.D. Uchic and C. Woodward

Air Force Research Laboratory, Materials and Manufacturing Directorate, AFRL/RX Wright-Patterson AFB, OH

*UES, Inc., Dayton, OH

#UTC, Dayton, OH

Abstract

We extend our recent work where a screw dislocation in FCC Ni was found to spontaneously attain a low-energy partially cross-slipped configuration upon intersecting a forest dislocation [1]. Using atomistic (molecular statics) simulations with embedded atom potentials, we evaluate the activation barrier for a dislocation to transform from fully residing on the glide plane to fully residing on the cross-slip plane intersecting a forest dislocation. The activation energies were obtained by determining equilibrium configurations (energies) when variable pure tensile or compressive stresses are applied along the [111] direction on the partially cross-slipped state. We show that the activation energy is a factor of 3 - 6 lower than that for cross slip in isolation via the Escaig process. Further, the activation barrier for cross-slip at these intersections is shown to be linearly proportional to (d/b)ln(d/b), as in the Escaig process, where 'd' is the Shockley partial dislocation spacing and „b' is the Burgers vector of the screw dislocation. These results suggest that cross-slip should be preferentially observed at selected screw dislocation intersections in FCC materials.

Keywords: Cross-slip; Activation analysis, Atomistic simulations; Nickel; Escaig stresses

1.0 Introduction

There is an increasing recognition of the need to incorporate physics-based models of deformation in design of structural components. While models for predicting yield strength and creep behavior are beginning to incorporate significant physics, models for fatigue and ultimate strength remain mostly empirical. This is because strain-hardening and fatigue resistance are highly influenced by dislocation micromechanisms, for example cross-slip, and including physics-based cross-slip processes in mesoscale simulations (e.g. dislocation dynamics) has been difficult. The early work of Escaig remains the most widely cited and used model for cross-slip [2-5]; however, this model poses several difficulties with respect to quantitative simulations. The model is highly sensitive to choice of parameters that have thus far been difficult to obtain. For example, the constriction width required for cross-slip is unknown but significantly influences the enthalpy of the cross-slip process [6]. This difficulty has led to an ad-hoc postulate that obstacles always exist in materials which enable sufficient dislocation core constriction under stress thereby ensuring cross-slip [2]. Aside from being a presumption, this forces cross-slip models (particularly for single crystals) to make arbitrary assumptions about the dislocation obstacle spacing. Advances in atomistic simulations make it possible to gain insights into the cross-slip process and may serve to inform mesoscale simulations to accurately capture the atomic-level physics of that dislocation process. Such an insight was realized in our recent work[1], where the possibility of cross-slip at dislocation-dislocation intersections was selectively examined using large-scale atomistic simulations

that contain more than one dislocation. *A glide dislocation that intersects a pair of forest dislocations was modeled and several conditions were shown to exist where cross-slip can nucleate easily.* This provides a better physical basis for cross-slip and means to incorporate realistic cross-slip evolution in larger-scale, discrete dislocation-dynamics simulations. Further, this may lead to a realistic statistical representation of cross-slip during monotonic or cyclic deformation. However, the prior work did not explore the size and nature of the activation barrier for the dislocation transformation at intersections.

In this work we show that a finite energy barrier exists for cross slip at an intersection, but that it is much smaller than that currently understood from analyses of the Escaig process. Molecular statics simulations were used to determine the saddle point configuration and activation energy by changing the extent of partial dislocation cross-slip using an applied stress. The applied stresses were compressive or tensile along the [111] direction on the partially cross-slipped dislocation structures obtained in prior work [1]. The screw-character dislocation under study had a $\frac{1}{2}[1\bar{1}0]$ Burgers vector and the intersecting dislocation had the $\frac{1}{2}[\bar{1}01]$ Burgers vector on the $(1\bar{1}1)$ plane and a 120^{o} line orientation of [0-1-1]. Section 2 describes the simulation technique and the interatomic potential used for the simulations. Section 3 presents a review of the core structures obtained from atomistic simulations for this specific intersection [1], the effect of applied stresses along the [111] direction on the partially cross-slipped core structure, the identification of the saddle point configuration and a determination of the energies of the activated state for cross-slip. Finally, Sections 4 and 5 give a discussion and summary of the results respectively.

2.0 Simulation technique

The atomistic simulations described here employed the 3-dimensional (3d) parallel molecular dynamics code, LAAMPS [7], developed at Sandia National Laboratory. A schematic of the simulation cell used in the atomistic simulations is given in Figure 1. The simulation cell is a rectangular parallelepiped having the x-axis oriented along $[1\bar{1}0]$, y-axis along $[11\bar{2}]$ and the z-axis along [111]. The dimensions of the simulation cell are 62.0 nm along the x-axis and 31.5 nm along both the y- and z- axes corresponding to a simulation cell of 5,405,160 atoms. The partially cross-slipped core structures obtained for the screw ($1/2[\bar{1}10]$ Burgers vector) – 120^o ($1/2[\bar{1}01]$ Burgers vector, $[0\bar{1}\bar{1}]$ line direction) intersection in reference 1 were subjected to uniform compressive or tensile stresses applied along the [111] direction. Under such a state of stress, there are no resolved shear stresses acting along the Burgers vector direction for either the screw or the 120^o dislocation. Also, there are no applied Escaig stresses acting on the edge components of the screw-character dislocation on the (111) glide plane. However, there are Escaig stresses acting on the edge components of the screw dislocation on the cross-slip $(11\bar{1})$ plane as well as the forest dislocation on the $(1\bar{1}1)$ plane. Fixed boundary conditions were applied along all three directions and energy minimization was performed using the conjugate gradient technique. Such results were analyzed to obtain the energy differences between the fully-on-glide-plane core structure, fully-on-cross-slip plane core structure and, the activated structures for this intersection.

The approach used to obtain activation energies for transformation from one core structure to another is as follows: As the stress is varied, the relative magnitudes of Escaig stresses on the glide plane and cross-slip plane change, thus affecting a variation

in the length of the partially cross-slipped region of the screw-character dislocation. Note that stabilizing each configuration requires manipulation of stresses before, after and at the inflection point in the energy-distance coordinate. By releasing the stress from the stabilized state, the configuration was allowed to "fall" towards either side of the saddle point configuration. This process allowed the identification of the saddle point configuration (within the energy error of the technique). Once identified, the absolute energy of this configuration without the applied stress is calculated by freezing a small volume of atoms near the core transformation region and then minimizing the energy of all other atoms in the cell. This gives an upper bound for the energy of the saddle point. The activation energy is obtained by subtracting the energy of the fully-glide-plane-spread core configuration from that of the saddle point configuration. The primary error in this calculation arises from the fact that an arbitrary number of atoms are kept fixed while obtaining the energy of the saddle point configuration without applied stress.

2.1 Interatomic Potential

The embedded atom potentials used for the simulations are the potentials developed for FCC Ni by Angelo, Moody and Baskes [8] based on the Voter and Chen format (Angelo), as well as the two Ni potentials developed based on the Voter and Chen format which Rao et.al. used in their bulk cross-slip simulations, vni and vnih [9]. Table 1 gives the lattice parameter, cohesive energy, elastic constants and stacking fault energy for each of the potentials. The three Ni potentials used in the simulations give almost identical elastic constants, cohesive energy and lattice parameter, whereas the stacking fault energy given by the potentials varies from 60 – 120 mJ/m^2. The Shockley partial spacing

width, d, for the screw dislocation varies from d/b = 5 for potential vnih to d/b =8 for potential vni. The Angelo potential gives a d/b ratio of approximately 6. This allows a determination of cross-slip activation energy as a function of d/b ratio.

2.2 Depiction of core structures

In order to illustrate the relaxed screw dislocation geometries we take advantage of the increase in atomic energy produced by the strain field of the partial dislocations. By plotting the atoms having assigned energies within LAAMPs of greater than -4.42 or -4.40 eV (the energy of atoms in the stacking fault region) the partial dislocations can be imaged easily, even for these large simulation cells. In order to illustrate the cross-slipped-segment products of the screw dislocation the positions are shown in a [111] as well as a $[11\bar{2}]$ projection. For the $[11\bar{2}]$ projection, segments spread on the initial (111) plane appear as a single line and cross-slipped segments (i.e. on a $(11\bar{1})$ plane) appear as a pair of partials separated by a stacking fault.

3.0 Review of atomistic core structures for the 120^o intersection

Figures 1- 3 depict the [111] and $[11\bar{2}]$ projections (i.e. the „x-y' and „x-z' planes) of the various core structures obtained for the screw dislocation – 120^o dislocation intersection, discussed in reference 1, obtained using the Angelo EAM potential. The starting configurations and boundary conditions are discussed in detail in the literature [1]. Figure 1 illustrates a screw dislocation fully on the glide (111) plane and constricted (i.e. Stroh constrictions [10]) at both the intersections around one of the Shockley partials of the 120^o ½$[\bar{1}01]$ dislocation residing on the $(1\bar{1}1)$ plane. Figure 2 depicts two of the core structures obtained for the screw dislocation -120^o dislocation intersection, Lomer-

Cottrell lock configurations (LC1 and LC2) in the [111] and [$11\bar{2}$] projections. After relaxation, figures 2a and 2b, the screw dislocation fully resides on the cross-slip ($11\bar{1}$) plane. In figure 2b, as in figure 1, the screw dislocation is constricted at both the intersections around one of the Shockley partials of the 120° ½[$\bar{1}$01] dislocation residing on the ($1\bar{1}1$) plane. In figure 2a, the a/6[$\bar{1}$12] Shockley partial of the screw dislocation combines with the a/6[$1\bar{2}\bar{1}$] Shockley partial of the 120° dislocation to form an extended node resulting in a short segment having Burgers vector of the type 1/6[$0\bar{1}1$] (e.g. a Lomer-Cottrell barrier). At the other end of the Lomer-Cottrell barrier, the screw dislocation is constricted to form one half of a Stroh constriction. Figure 3 shows the [111] and [$11\bar{2}$] projections for two of the core structures obtained for the screw dislocation - 120° dislocation intersection, identified as Partially Cross-Slipped Locks (PCS1 and PCS2). In both cases, the screw dislocation is partially on the glide (111) plane and partially on the cross-slip ($11\bar{1}$) plane. In figure 3a, as in figure 1, the screw dislocation is constricted at both the intersections (negative constrictions [9,11]) around one of the Shockley partials of the 120° ½[$\bar{1}$01] dislocation residing on the ($1\bar{1}1$) plane. Since the core is in the partially cross-slipped state, a companion positive constriction [9, 11] forms between the intersections. In figure 3b, as in figure 2b, a/6[$\bar{1}$12] Shockley partial of the screw dislocation combines with the a/6[$1\bar{2}\bar{1}$] Shockley partial of the 120° dislocation to form an extended node resulting in a short segment having Burgers vector of the type 1/6[$0\bar{1}1$] (e.g. a Lomer-Cottrell barrier). At the other end of the Lomer-Cottrell barrier, the screw dislocation is constricted to form one half of a negative constriction and is cross-slipped onto the glide (111) plane. Since the core is in the

partially cross-slipped state, a companion full positive constriction [9, 11] forms between the intersections.

3.1 Schematic description of the energy well

Figure 4 gives a schematic plot of the energy of the screw dislocation configuration at the intersection as a function of the length of screw dislocation cross-slipped onto the cross-slip plane in between the 120^o intersecting dislocations. Previous molecular statics simulation results [1] show that there are local minima in the energy curve when: the screw dislocation length on cross-slip plane goes to zero (fully-glide state), the entire screw dislocation length is on the cross-slip plane (fully-cross-slip state), and when approximately half the screw dislocation length between the intersections is on the cross-slip plane (partial-cross-slip state). Two local maxima are expected for the energy versus state curve, in between the fully-glide and partial-cross-slip state and the fully-cross-slip and partial-cross-slip state. Starting from the partial-cross-slip state, application of increasing Escaig stresses on the configuration are used to drive the screw dislocation up the energy well until a point of inflexion (e.g. the first derivative of the energy curve and the stress is a maximum). For stresses slightly above the point of inflexion in the energy curve, the screw dislocation will collapse to either the fully-glide or fully-cross-slip state. The work done by the Escaig stresses up to the inflexion point gives the energy required for the screw dislocation to transfer from the partially-cross-slipped state to the fully-glide-plane or fully-cross-slip-plane states. The maximum Escaig stresses under which the partial-cross-slipped state is stable are given by the maximum in the first derivative of this energy profile. The following procedure was used to determine the local maxima,

that is the activated state for transferring the screw dislocation from fully-glide-plane or fully-cross-slip-plane states to the partially-cross-slipped state in the energy curve. Partially-cross-slipped states, under Escaig stresses slightly above the maximum in first derivative of the energy curve, are relaxed and stopped at different points along the energy curve and the Escaig stresses relaxed back to zero. Depending on the initial value of the Escaig stress and the position on the activation surface, under zero stress the screw dislocation configuration will collapse to one of the three possible minimum energy states: partially-cross-slipped, fully-glide-plane or fully-cross-slipped. The point at which the screw dislocation transitions from relaxing to the partially-cross-slipped state to relaxing to fully-glide-plane or fully-cross-slipped-plane states is identified as the maxima in the energy curve or the activated state for cross-slip. The energy of this configuration relative to the fully-glide-plane or fully-cross-slip-plane states is evaluated by using 2 relaxation techniques from the activated configuration, which are described in section 3.4 below.

3.2 Behavior of cores PCS1 and PCS2 under stresses

Figure 5 gives the relaxed core structures in the $[11\bar{2}]$ projection for the screw – 120^o intersection (core structure PCS1) for uniform compressive applied stresses of 250, 500, 750, 1000, 1100 and 1150 MPa along the [111] direction, obtained using the Angelo EAM potential. For the 1150 MPa case, an additional increment of 50 MPa compressive stress was applied on the relaxed 1100 MPa compressive stress configuration. With increasing compressive applied stress, the amount of cross-slipped screw segment in between the two intersecting 120^o dislocations monotonically increases until a stress of

1100 MPa is reached. When the compressive applied stress is slightly increased from 1100 to 1150 MPa, the screw dislocation in between the intersections suddenly collapses to core structure LC2, fully residing on the cross-slip $(11\bar{1})$ plane. For compressive applied stresses, the effective stacking-fault energy on the cross-slip $(11\bar{1})$ plane decreases by an amount equal to $\tau_e b_e$, where $\tau_e = S\sigma_c$, S is the Schmidt factor acting on the edge component of the Shockley partials on the cross-slip $(11\bar{1})$ plane, σ_c is the applied compressive stress along the [111] direction and b_e is the magnitude of the edge component, = 0.071 nm. Similarly, figure 6 gives the relaxed core structures in the $[11\bar{2}]$ projection for the screw – 120^o intersection (core structure PCS1) for uniform tensile applied stresses of 250, 500, 750, 1000 and 1050 MPa along the [111] direction, again obtained using the Angelo EAM potential. As before, for the 1050 MPa case, a slight additional increment of 50 MPa tensile stress was applied on the relaxed 1000 MPa tensile stress configuration. In this case, the amount of cross-slipped segment in between the two intersecting 120^o dislocations montonically decreases until a stress of 1000 MPa is reached. When the tensile applied stress is slightly increased from 1000 to 1050 MPa, the screw dislocation in between the intersections suddenly relaxes to core structure Gl1, fully residing on the glide (111) plane. For tensile applied stresses, the effective stacking-fault energy on the cross-slip $(11\bar{1})$ plane increases by an amount equal to $\tau_e b_e$, where $\tau_e = S\sigma_t$, σ_t is the applied tensile stress along the [111] direction. Similar behavior was observed for core structure PCS2. In this case, when the applied stress was compressive, core structure PCS2 relaxes to core structure LC1, when the compressive stress was increased from 650 to 700 MPa. Similarly, for tensile applied stresses, core

structure PCS2 realxes to core structure Gl1, when the applied tensile stress was increased from 1150 to 1200 MPa.

3.3 Analysis of cores PCS1 and PCS2 under applied stresses

Figures 7a and 7b illustrate the change in length of the cross-slipped segment in between the two intersecting 120^o dislocations (x-axis) versus the change in effective stacking-fault energy [y-axis] due to the applied compressive or tensile stresses along the [111] direction, for initial core structure PCS1, obtained using the Angelo EAM potential. Figures 7a and 7b clearly show that for a certain critical increase or decrease in stacking-fault energy, $\delta\gamma$, the core structure for the intersection collapses to either LC2, fully residing on the cross-slip plane (compressive stress) or Gl1, fully residing on the glide plane (tensile stress). The work done by the applied stresses up to the critical point is given by the area under the curve up to the critical point, multiplied by the Shockley partial spacing (estimated to be 6b, where b is the magnitude of the Burgers vector of the screw dislocation [9]) and is equal to the energy difference between the activated states and the partially cross-slipped state, PCS1, $\delta E_{act\text{-}PCS1}$. This is determined to be 0.68 eV for the activated state on the compressive side and 1.44 eV for the activated state on the tensile side. The Escaig stresses required for transferring the dislocation from the partially-cross-slipped state (PCS1), to the fully-glide-plane state (on the tensile side, Gl1), is 314 MPa and, to the fully-cross-slipped state (LC2) is 346 MPa.

Similarly, figures 8a and 8b show the change in length of the cross-slipped segment in between the two intersecting 120^o dislocations (x-axis) versus the change in effective stacking-fault energy [y-axis] due to the applied compressive or tensile stresses along the

[111] direction, for initial core structure PCS2, obtained using the Angelo EAM potential. The Escaig stresses required for transferring the dislocation from the partially cross-slipped state (PCS2) to the fully-glide-plane state (on the tensile side, GL1), is 361 MPa and to the fully-cross-slipped state (LC1) is 204 MPa.

3.4 Determination of cross-slip activation energy

To determine the activation energy for cross-slip from the fully-glide-plane state (Gl1) to the partially-cross-slipped state (PCS1), the simulation having 1050 MPa tensile stress applied on the partially-cross-slipped state PCS1, was stopped after varying amounts of relaxation and the applied stress relaxed back to zero. Conjugate gradient minimization after the stress is relaxed back to zero indicated whether the core relaxes to the partially-cross-slipped state (PCS1) or the fully-glide-plane state (Gl1). The configuration at which the relaxation transitions from relaxing to PCS1 to relaxing to Gl1, is taken to be the activated state for cross-slip from Gl1 to PCS1. Figure 9 gives the structure of the activated state in the $[11\bar{2}]$ projection for the screw – 120^o intersection (core structure PCS1), obtained using the Angelo potential, which gives a stacking-fault energy of 90 mJ/m^2. Figure 9a shows that in the activated configuration, a small portion of the screw dislocation near the intersection, of length ~1.5 d, resides on the cross-slip plane. The attractive interaction between the negative and positive constrictions goes to zero at a separation distance of 1.5 d, beyond which it becomes repulsive, in the presence of an intersecting dislocation. This behavior is significantly different from typical Escaig process for cross slip where the attractive interaction between the constrictions only goes to zero at an infinite separation distance [3-5]. Similar analysis was performed to

determine the activation energy for cross slip from the fully-cross-slip-plane state (LC2) to the partially-cross-slipped state (PCS1). In this case the simulation having 1150 MPa compressive stress applied on the partially cross-slipped state PCS1 was stopped after varying amounts of relaxation and the applied stress relaxed back to zero. Conjugate gradient minimization after the stress is relaxed back to zero indicated whether the core relaxes to the partially-cross-slipped state (PCS1) or the fully-cross-slip-plane state (LC2). The configuration at which the relaxation transitions from relaxing to PCS1, to collapsing to LC2, is taken to be the activated state for cross-slip from LC2 to PCS1. Figure 9b shows that in the activated configuration, a small portion of the screw dislocation near the intersection, of length ~d, resides on the glide plane. The attractive interaction between the negative and positive constrictions goes to zero at a separation distance of d beyond which it becomes repulsive, in the presence of an intersecting dislocation. Such a behavior is significantly different from the standard Escaig process.

The activation energy for cross-slip from state Gl1 to state PCS1, $\delta E_{Gl1\text{-}PCS1}$ was determined using two different relaxation techniques from the identified activated configuration. In the first technique, the energy was determined for relaxation from the activated state, to state Gl1, under an applied tensile stress of 1050 MPa along the [111] direction. This energy was corrected for two factors to obtain the activation energy for cross-slip: a) work done by the applied Escaig stresses in collapsing the activated configuration (of the order of 0.2 eV) and, b the increase in energy of the activated configuration due the applied Escaig stresses (of the order of 0.4 eV). For the second technique, the activated state was relaxed to state Gl1 having zero applied stress, with and without atoms within a cube of size 1.2 nm centered at the positive constriction of the

activated state fixed. The difference in relaxation energies between the two types of simulations was taken to be the activation energy for cross slip from Gl1 to PCS1. The results for the cross-slip activation energy obtained using these two techniques of relaxation were within 0.2 eV of each other and, are taken to be representative of the error in the determination of the activation energy for cross slip using this procedure. Similar simulations and analysis were performed to determine the activation energy for cross-slip from Gl1 to PCS1 using two other Ni EAM potentials, vni and vnih. Also, similar simulations and analysis were performed to determine the activation energy for cross slip from the fully-cross-slip-plane state (LC2) to the partially-cross-slipped state (PCS1) using all three EAM potentials, $\delta E_{LC2\text{-}PCS1}$. In this case, the two techniques of relaxation described before for determining the cross-slip activation energy gave values that differed by less than 0.1 eV. Figure 10 is a plot of the cross-slip activation energies for cross slip from state Gl1 to state PCS1, as well as from state LC2 to state PCS1, obtained using the three Ni EAM potentials, versus the parameter (d/b)ln(d/b) given by the potentials. Also plotted in figure 10 are the corresponding values for the cross-slip activation energy determined from simulations of the Escaig process [ref]. Figure 10 clearly shows that the cross-slip activation energy is linearly proportional to (d/b)ln(d/b) both at the intersection and for the Escaig-type process. The cross-slip activation-energy (from Gl1 to PCS1) values near the intersection are a factor of 3-4 lower than that for the Escaig process. Also, the cross-slip activation energy from the fully-cross-slip-plane state (LC2) to the partially-cross-slipped state (PCS1), is approximately a factor of 6 lower than that for the Escaig process. The $\delta E_{LC2\text{-}PCS1}$ values can be identified, by symmetry, as the cross-slip activation energy from the fully-glide plane-state to the

partially-cross-slipped state at a 120° screw dislocation intersection, where the intersecting forest dislocation has a 1/2<011> Burgers vector, $<10\bar{1}>$ line direction and resides on the $(1\bar{1}1)$ plane. This suggests that the cross-slip activation energy near an intersection is strongly dependent on the Burgers vector of the intersecting dislocation and could be a factor of 6 lower than that usually considered. To obtain the cross-slip activation energies dislocations intersecting forest dislocations in other FCC metals from Fig. 10, one has to scale by the elastic constants of the metal relative to that of Ni at the appropriate d/b ratio for that metal. Note that Fig. 10 shows that intersection cross-slip activation energies for typical FCC metals such as Ni, Cu and Au ranges from 0.3 – 0.7 eV. The activation volume for the cross-slip process with respect to applied Escaig stresses is given by the area of the cross-slipped portion of the screw character dislocation in the activated state (Fig. 9) multiplied by the magnitude of the edge component of the Burger's vector of the Shockley partials. From the simulations, values for this parameter range from $10 – 20b^3$ for cross-slip at screw dislocation intersections.

4.0 Discussion

The results of this work clearly show that cross-slip nucleation at screw dislocations intersecting forest dislocations is relatively easy, having an activation energy that is a factor of 3-6 lower than that for the Escaig process. This is an important result since the probability of dislocation intersections is relatively large as compared to other mechanisms of obstacle induced cross-slip, like cross-slip at screw dipoles, jogs, and surfaces [13-15]. Further, cross-slip at screw dipoles, jogs and surfaces is athermal only under specific conditions [13-15]. The current result rationalizes the profuse nature of

cross slip in FCC crystals, unlike the current models of thermally-activated cross slip that require high stress to provide a self-consistent explanation. This finding should allow higher-level mesoscale models of dislocation behavior to better represent the cross-slip process without resort to ad hoc assumptions about obstacles. It should be noted that since a molecular statics technique has been used in this work, the cross-slip activation-energy values reported in this manuscript are expected to be upper bounds. A more sophisticated molecular dynamics reaction pathway technique [16] might provide more accurate values for the activation energies of cross slip near forest dislocation intersections.

The new cross-slip nucleation model has a variety of implications for crystal plasticity in FCC materials. For example, within the present mechanism, the frequency of cross-slip should scale with the forest dislocation density. The growth of such nuclei should depend upon the relative magnitude of local stresses on the glide plane and the cross-slip plane at the partially cross-slipped screw-dislocation intersection region. Such behavior of the partially cross-slipped core under different modes of applied stress could be studied using atomistic simulations as well as dislocation dynamics simulations. Similar activation analysis using atomistic simulations must be performed for other intersections (varying line direction of the intersecting dislocation) on the $(1\,\bar{1}\,1)$ plane that form Glide, Lomer-Cottrell or Hirth locks to determine the dependence of the activation energy for cross-slip on the line direction as well as the Burger's vector of the intersecting forest dislocation. Also, it would be instructive to perform activation analysis using atomistic simulations of these screw-dislocation intersection core structures for other FCC materials having different stacking fault energies (i.e. Al and

Cu) to verify the results in Ni. The intersection mechanism of cross-slip nucleation should also be implemented in 3d dislocation dynamics simulations as an alternative to Escaig's model for FCC materials. Finally, it would be instructive to revisit the Bonneville and Escaig experimental results on cross-slip in FCC Cu in light of the new intersection mechanism for cross-slip nucleation [2, 17].

According to Washburn [18], double-intersection cross slip, where the segment that has been pulled into the cross-slip plane soon encounters another attractive intersection that brings it back onto another primary glide plane, provides a reasonable mechanism for dislocation multiplication and the growth of slip bands at low temperatures. Naturally, such a mechanistic process must be demonstrated via modern simulation methods. Also, classical theories of strain-hardening assume that dislocation storage in Stage II of single-crystal FCC materials is a result of junction formation [19] or, 2-dimensional concave loop formation [20] as the gliding dislocation traverses through an array of forest dislocation obstacles on its glide plane. However, one of the major problems in classical strain-hardening models is to explain how the generation of a three-dimensional network of stored dislocations occurs as a consequence of two-dimensional glide [20]. We note that the intersection cross-slip nucleation mechanism for dislocation storage may provide a convenient mechanism of generating a three-dimensional network of stored dislocations from two-dimensional glide.

Finally, the anomalous flow behavior of intermetallics (i.e. Ni_3Al) has thus far been modeled using core transformations that require thermal activation. Here again, the key issue has been that constriction energies are prohibitively high [3,4,21]. The possibility of the core transformation in the presence of interaction with other dislocations provides

a novel mechanism to consider and explore in rationalizing the flow anomaly of these types of materials.

5.0 Summary

Atomistic simulations were conducted to identify the saddle-point configuration and thus the activation energy for cross slip of a screw dislocation in the presence of a pair of forest dislocations. The approach involved the use of external stress along [111] to vary the segment length for a partially cross slipped ½$[1\bar{1}0]$ screw dislocation intersecting a pair of 120° ½$[\bar{1}01]$ Burgers vector, $<0\bar{1}\bar{1}>$ line direction dislocations residing on the $(1\bar{1}1)$ plane. The simulations in this work show that the nucleation of cross-slip at dislocation-dislocation interactions is significantly more probable than the Escaig process, having an activation barrier that is a factor of 3 - 6 lower. Further, this work shows that atomistic simulations can be used to identify types of interactions that result in cross-slip and these results in turn may be used in higher-level mesoscale simulations. Summarizing the results: equilibrium partially cross-slipped core structures under applied compressive or tensile stresses along the [111] direction were determined using atomistic simulations. Beyond a critical stress, the equilibrium configurations relax to a core structure that is either fully on the glide plane for tensile stresses or fully on the cross-slip plane for compressive stresses.

1) The activation barrier for cross-slip from the fully-glide-plane state (Gl1) to the partially-cross-slipped state (PCS1), $\delta E_{Gl1\text{-}PCS1}$ at these intersections, is determined to be a factor of 3-4 lower than that for the Escaig process. While the new cross slip mechanism has a lower activation energy it has the same linear relationship to (d/b)ln(d/b) as the

Escaig process. The activation barrier for cross-slip from the fully-cross-slip-plane state (LC2) to the partially-cross-slipped state (PCS1), $\delta E_{LC2\text{-}PCS1}$ at these intersections, is determined to be approximately a factor of 6 lower than for the Escaig process. These $\delta E_{LC2\text{-}PCS1}$ values, by symmetry, are identified as the activation barrier for cross-slip from the fully-glide-plane state to the partially-cross-slipped state at a 120^o screw dislocation intersection, where the intersecting dislocation has a ½<011> Burgers vector, $<10\bar{1}>$ line direction and resides on the $(1\bar{1}1)$ plane.

2) Cross-slip activation-energy values near forest dislocation intersections in typical FCC metals like Ni, Cu and Au range from 0.3 – 0.7 eV.

ACKNOWLEDGEMENT

The authors acknowledge use of the 3d molecular dynamics code, LAAMPS, which was developed at Sandia National Laboratory by Dr. Steve Plimpton and co-workers. This work was supported by the AFOSR under USAF contract No.FA8650-04-D-5235, and by a grant of computer time from the DOD High Performance Computing Modernization Program, at the Aeronautical Systems Center/Major Shared Resource Center. The work was performed at the U.S. Air Force Research Laboratory, Materials and Manufacturing Directorate, Wright-Patterson AFB.

REFERENCES

1. Rao S, Dimiduk DM, El-Awady J, Parthasarathy TA, Uchic MD, and Woodward C. 2009, accepted for publication in Phil. Mag.

2. Bonneville J, and Escaig B. Acta Metallurgica; 1979; 27: 1477.

3. Escaig B. Proceedings of the Battelle Colloquium on Dislocation Dynamics, edited by A.R. Rosenfield, G.T. Hahn, A.L. Bement Jr., and R.I. Jaffee (New York : McGraw-Hill); 1968: 655.

4. Puschl W. Prog. Mater. Sci.; 2002; 47: 415.

5. Caillard D, and Martin JL. „Thermally activated mechanisms in Crystal Plasticity'; 2003; Pergamon-Elsevier, Amsterdam.

6. Saada G. Mater.Sci. and Engr.; 1991; A137: 177.

7. Plimpton SJ. J.Comp.Phys.; 1995; 117: 1.

8. Angelo JE, Moody NR, and Baskes MI. Modell. Simul. Mater. Sci. Eng.; 1995; **3**: 289.

9. Rao S, Parthasarathy TA and Woodward C. Phil.Mag.A; 1999; 79: 1167.

10. Stroh AN. Phil. Mag.; 1959; 3: 625.

11. Rasmussen T, Jacobsen KW, Leffers T, and Pedersen DB. Phys.Rev.B; 1997; 56: 2977.

12. Martinez E, Marian J, Arsenlis A, Victoria M, and Perlado, JM. Jour. of the Mechanics and Physics of Solids; 2008; 56: 869.

13. Rao S, Dimiduk DM, Jaafar El-Awady, Parthasarathy T.A., Uchic MD, and Woodward C. to be published (2009).

14. Brown LM. Phil.Mag.A; 2002; 82: 1691.

15. Vegge T, and Jacobsen KW. J.Phys: Condens. Matter; 2002; 14: 2929.

16. Pendurti S, Jun S, Lee I and Prasad V. Appl.Phys.Ltrs; 2006; 88: 201908.

17. Bonneville J, Escaig B, and Martin JL. Acta Metallurgica; 1988; 36**:**1989.

18. Washburn J. Appl. Phys. Letters; 1965; 7: 183.

19. Devincre B, Hoc T and Kubin L. Science; 2008; 320: 1745.

20. Kocks UF, and Mecking H. Progress in Materials Science; 2003; 48(3): 102.

21. Parthasarathy TA, and Dimiduk D. Acta Mater.; 1996; 44: 2237.

Figure captions

Figure 1: [111] (X-Y plane) and $[11\bar{2}]$ (X-Z plane) projections of the core structure (Gl1) for a screw-120^0 intersection in FCC Ni from atomistic simulations. Atoms having an energy greater than the energy at a stacking fault are plotted. The axes dimensions are in units of Angstroms.

Figure 2: [111] (X-Y plane) and $[11\bar{2}]$ (X-Z plane) projections of the core structures (LC1 and LC2) for a screw-120^0 intersection in FCC Ni from atomistic simulations. Atoms having energies greater than the energy at a stacking fault are plotted. The axes dimensions are in units of Angstroms.

Figure 3: [111] (X-Y plane) and $[11\bar{2}]$ (X-Z plane) projections of the core structures (PCS1 and PCS2) for a screw-120^0 intersection in FCC Ni from atomistic simulations. Atoms having energies greater than the energy at a stacking fault are plotted. The axes dimensions are in units of Angstroms.

Figure 4: a) A schematic plot of the energy profile of the screw-dislocation configuration as a function of the length of the screw dislocation on the cross-slip plane in between the forest dislocation intersections. b) A schematic sketch of the $[11\bar{2}]$ projection of the screw-dislocation configuration in between forest dislocation intersections under applied Escaig stresses.

Figure 5: The $[11\bar{2}]$ projection of the equilibrium configurations of the partially cross-slipped core structure, PCS1, under uniform applied compressive stresses of 0, 250, 500, 750, 1000, 1100 and 1150 MPa applied along the [111] direction. Atoms having energies greater than the energy at a stacking fault are plotted. The axes dimensions are in units of Angstroms.

Figure 6: The $[11\bar{2}]$ projection of the equilibrium configurations of the partially-cross-slipped core structure, PCS1, under uniform applied tensile stresses of 0, 250, 500, 750, 1000and 1050 MPa applied along the [111] direction. Atoms having energies greater than the energy at a stacking fault are plotted. The axes dimensions are in units of Angstroms.

Figure 7: A plot of the increase or decrease in length of the cross-slipped segment in between the two intersecting 120^o dislocations (x-axis) versus the decrease or increase in effective stacking-fault energy [y-axis] due to the applied compressive or tensile stresses along the [111] direction, for initial core structure PCS1. The activation barrier for the transfer of the dislocation from the partially-cross-slipped state (PCS1) to the either the fully-cross-slip plane state (LC2) or the fully-glide plane state (Gl1) is also indicated.

Figure 8: A plot of the increase or decrease in length of the cross-slipped segment in between the two intersecting 120^o dislocations (x-axis) versus the decrease or increase in effective stacking-fault energy [y-axis] due to the applied compressive or tensile stresses

along the [111] direction, for initial core structure PCS2. The activation barrier for the transfer of the dislocation from the partially-cross-slipped state (PCS2) to the either the fully-cross-slip plane state (LC1) or the fully-glide plane state (Gl1) is also indicated.

Figure 9: The $[11\bar{2}]$ projection of the structure of the activated configuration for transfer of screw dislocation from a) state Gl1 to PCS1 (tensile side) and b) state LC2 to state PCS1 (compressive side) obtained using the Angelo EAM potential for Ni. The x axis is along the $[1\bar{1}0]$ direction and the y-axis is along the [111] direction. The axes dimensions are in units of Angstroms.

Figure 10: A plot of the activation energy for cross-slip from state Gl1 to state PCS1 ($\delta E_{Gl1\text{-}PCS1}$), as well as from state LC2 to state PCS1 ($\delta E_{LC2\text{-}PCS1}$), in Ni as a function of the parameter d/bln(d/b) given by the EAM potentials, Angelo, vni and vnih. Also shown are the corresponding cross-slip activation energy values for the Escaig process.

Property	Value (Angelo)	Value (vni)	Value (vnih)
a_0	0.352nm	0.35180789nm	0.35256848nm
C_{11}	2.46×10^{11} N/m^2	2.44×10^{11} N/m^2	2.44×10^{11} N/m^2
C_{12}	1.47×10^{11} N/m^2	1.49×10^{11} N/m^2	1.49×10^{11} N/m^2
C_{44}	1.25×10^{11} N/m^2	1.25×10^{11} N/m^2	1.19×10^{11} N/m^2
E_c	-4.45 eV	-4.43 eV	-4.43 eV
γ	.089 J/m^2	.059 J/m^2	.119 J/m^2

Table 1: Lattice parameter, a_0; Cohesive energy, E_c; Elastic constants C_{11}, C_{12} and C_{44}; and stacking fault energy, γ, given by the 3 Ni EAM potentials, Angelo, vni and vnih.

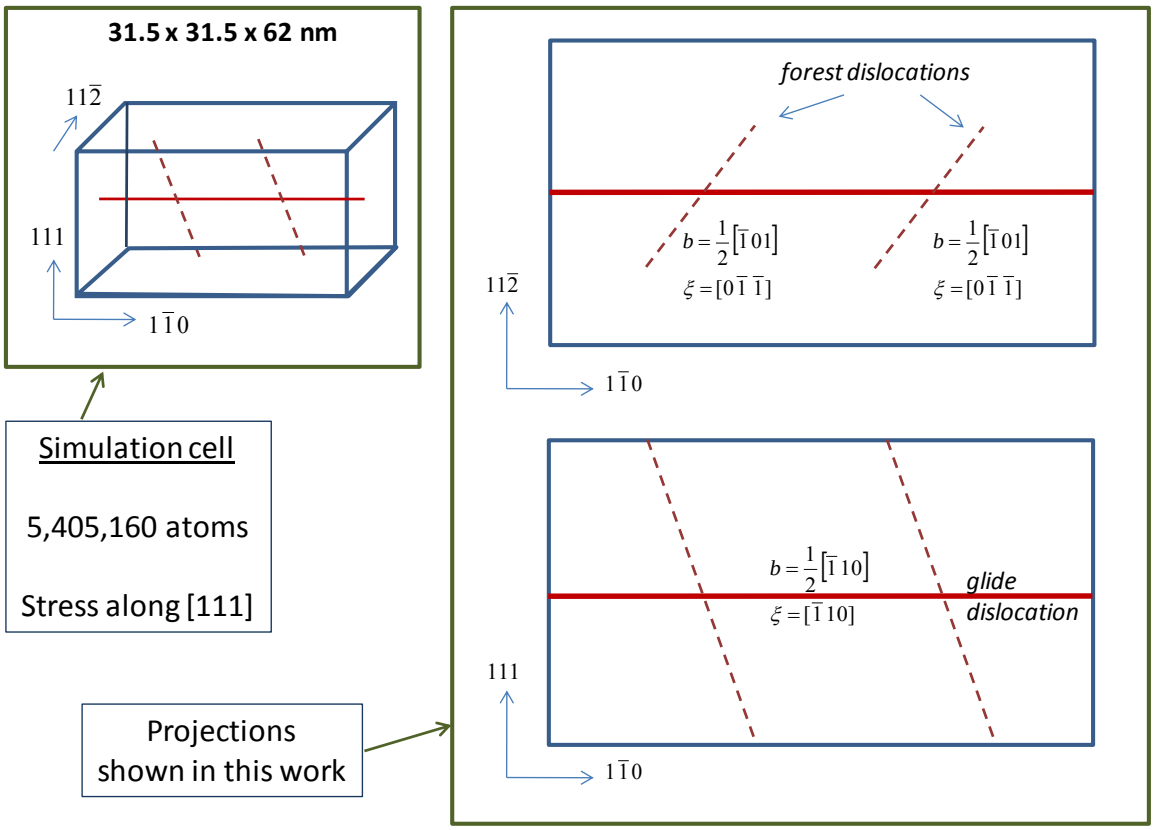
31.5 x 31.5 x 62 nm
$11\bar{2}$
111
$1\bar{1}0$
Simulation cell
5,405,160 atoms
Stress along [111]
Projections shown in this work
forest dislocations
$b=\frac{1}{2}[\bar{1}01]$
$\xi=[0\bar{1}\bar{1}]$
$b=\frac{1}{2}[\bar{1}01]$
$\xi=[0\bar{1}\bar{1}]$
$11\bar{2}$
$1\bar{1}0$
$b=\frac{1}{2}[\bar{1}10]$
$\xi=[\bar{1}10]$
glide dislocation
111
$1\bar{1}0$

Figure 1

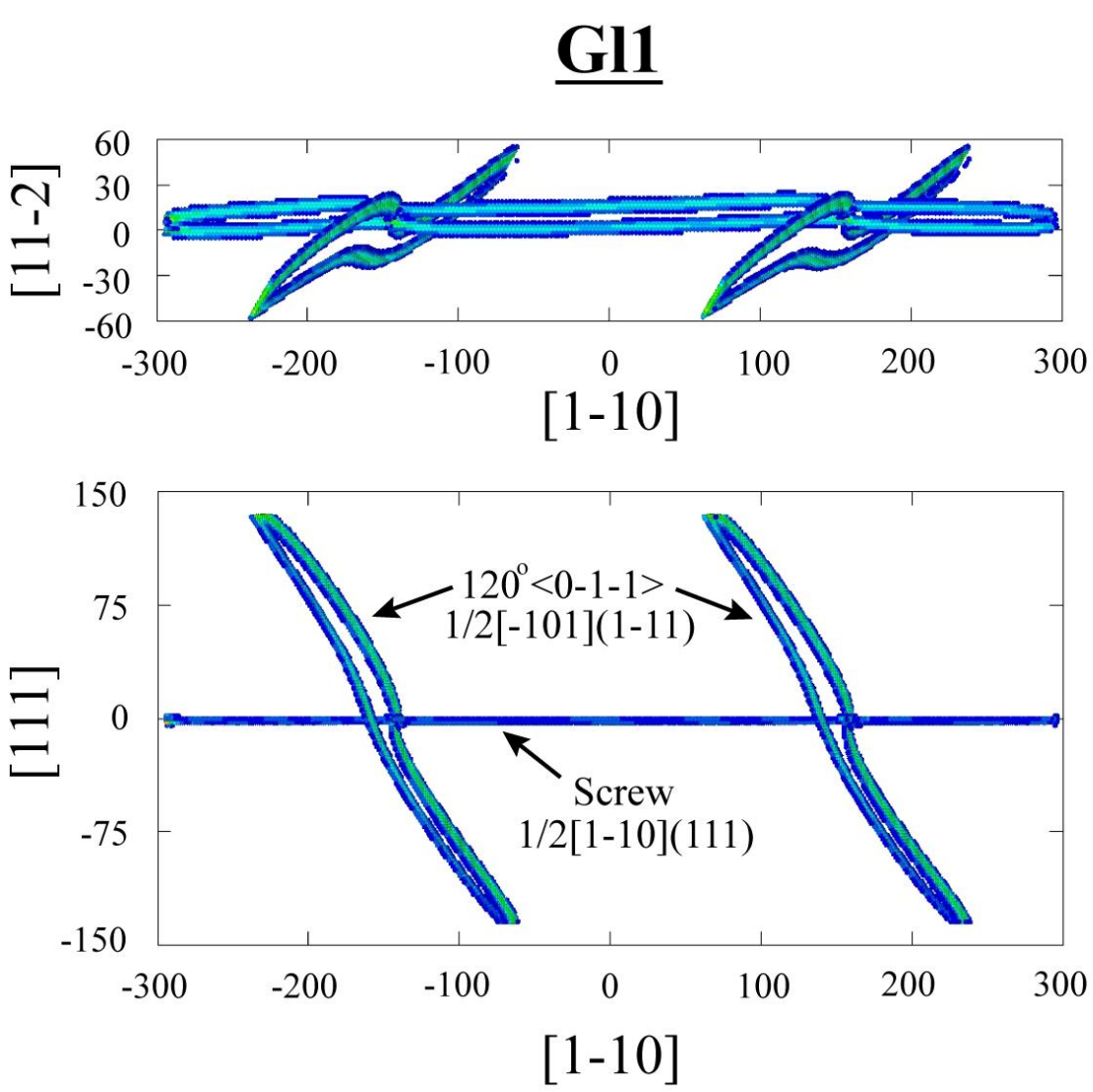
Gl1
[11-2]
60
30
0
-30
-60
-300
-200
-100
0
100
200
300
[1-10]
[111]
150
75
0
-75
-150
120°<0-1-1>
1/2[-101](1-11)
Screw
1/2[1-10](111)
-300
-200
-100
0
100
200
300
[1-10]

Fig.1:

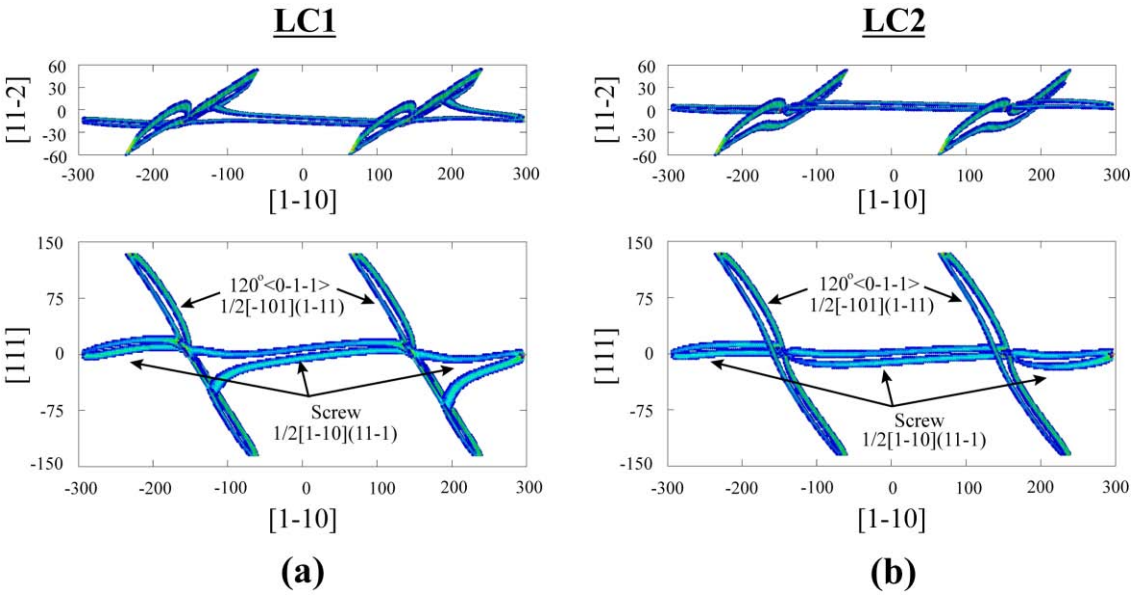

Fig.2:

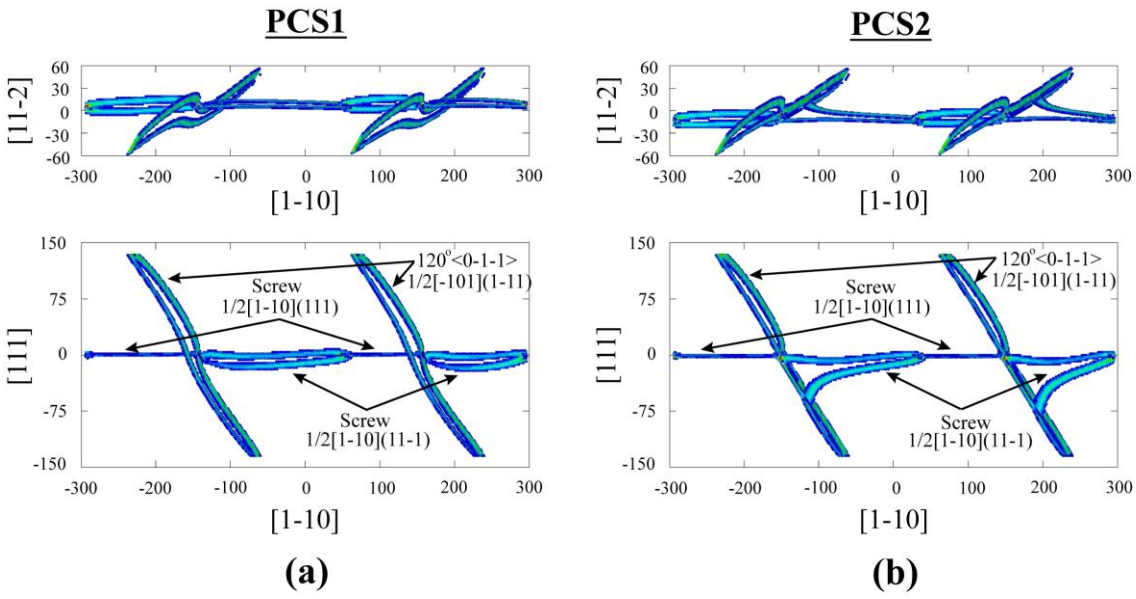
PCS1
PCS2
[11-2]
[1-10]
[111]
120°<0-1-1>
1/2[-101](1-11)
Screw
1/2[1-10](111)
Screw
1/2[1-10](11-1)
(a)
(b)

Fig. 3:

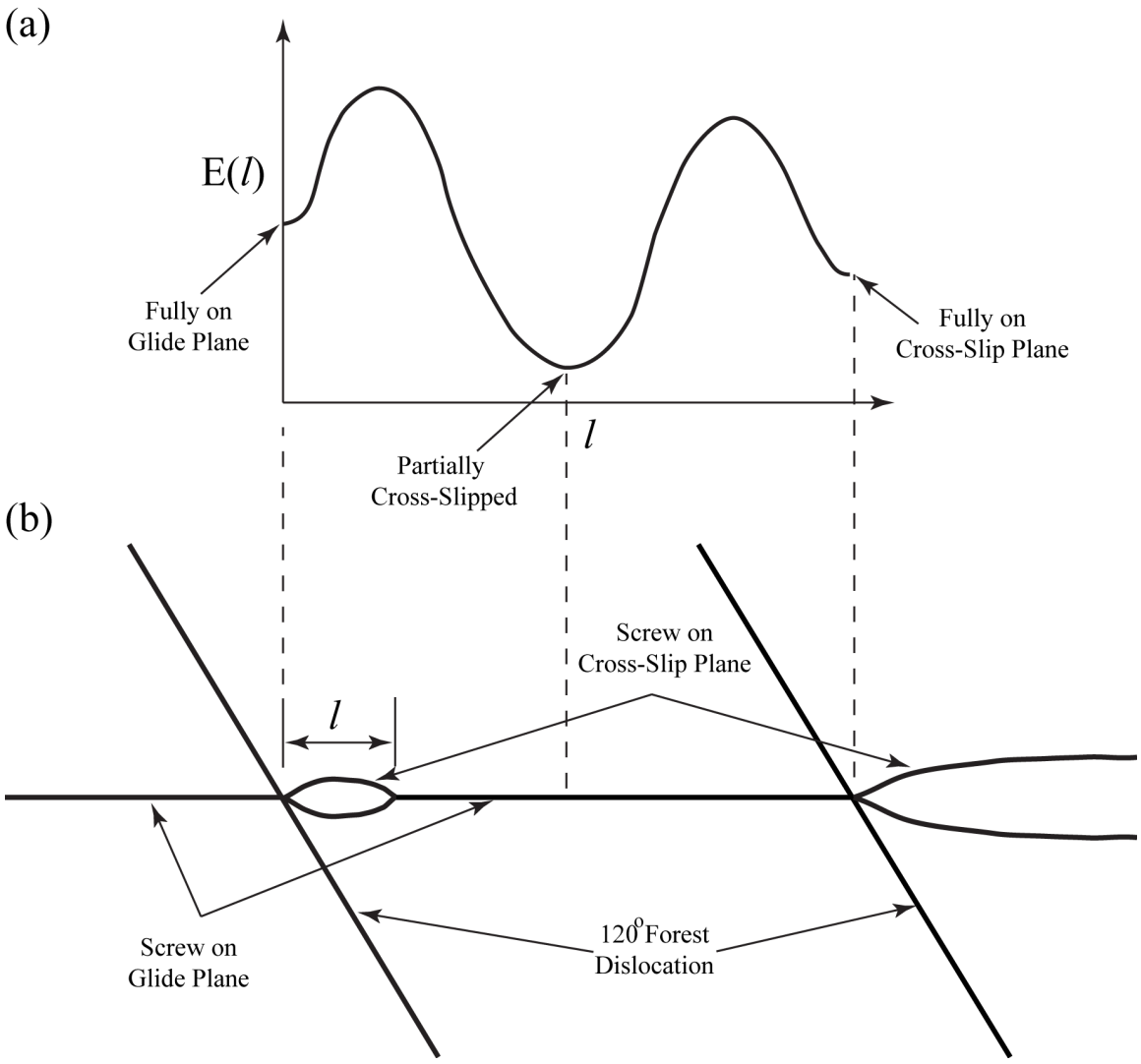
(a)
E(l)
Fully on
Glide Plane
Fully on
Cross-Slip Plane
l
Partially
Cross-Slipped
(b)
Screw on
Cross-Slip Plane
l
Screw on
Glide Plane
120° Forest
Dislocation

Fig.4:

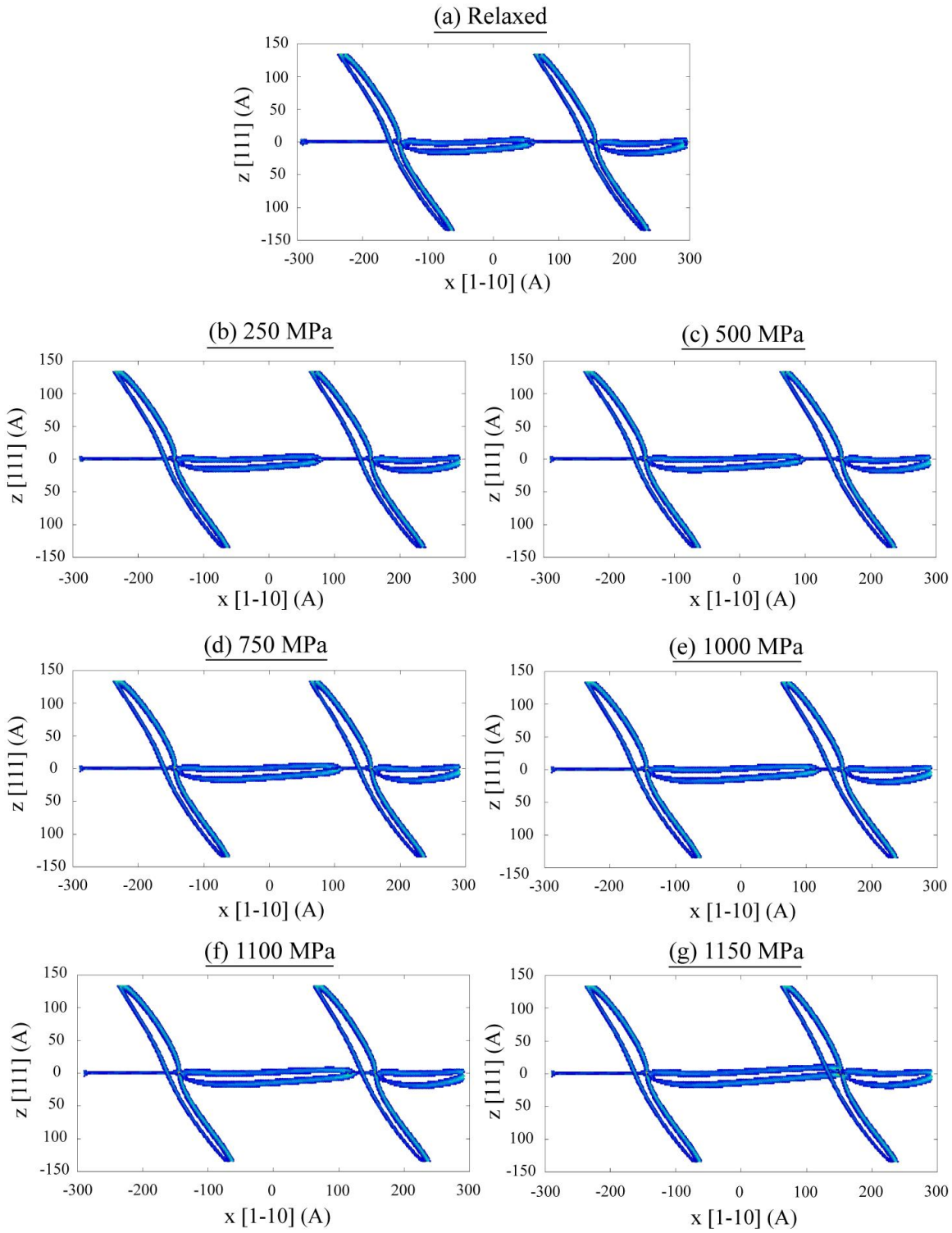
(a) Relaxed
(b) 250 MPa
(c) 500 MPa
(d) 750 MPa
(e) 1000 MPa
(f) 1100 MPa
(g) 1150 MPa
z [111] (A)
x [1-10] (A)
150
100
50
0
50
100
-150
-300
-200
-100
0
100
200
300

Fig. 5:

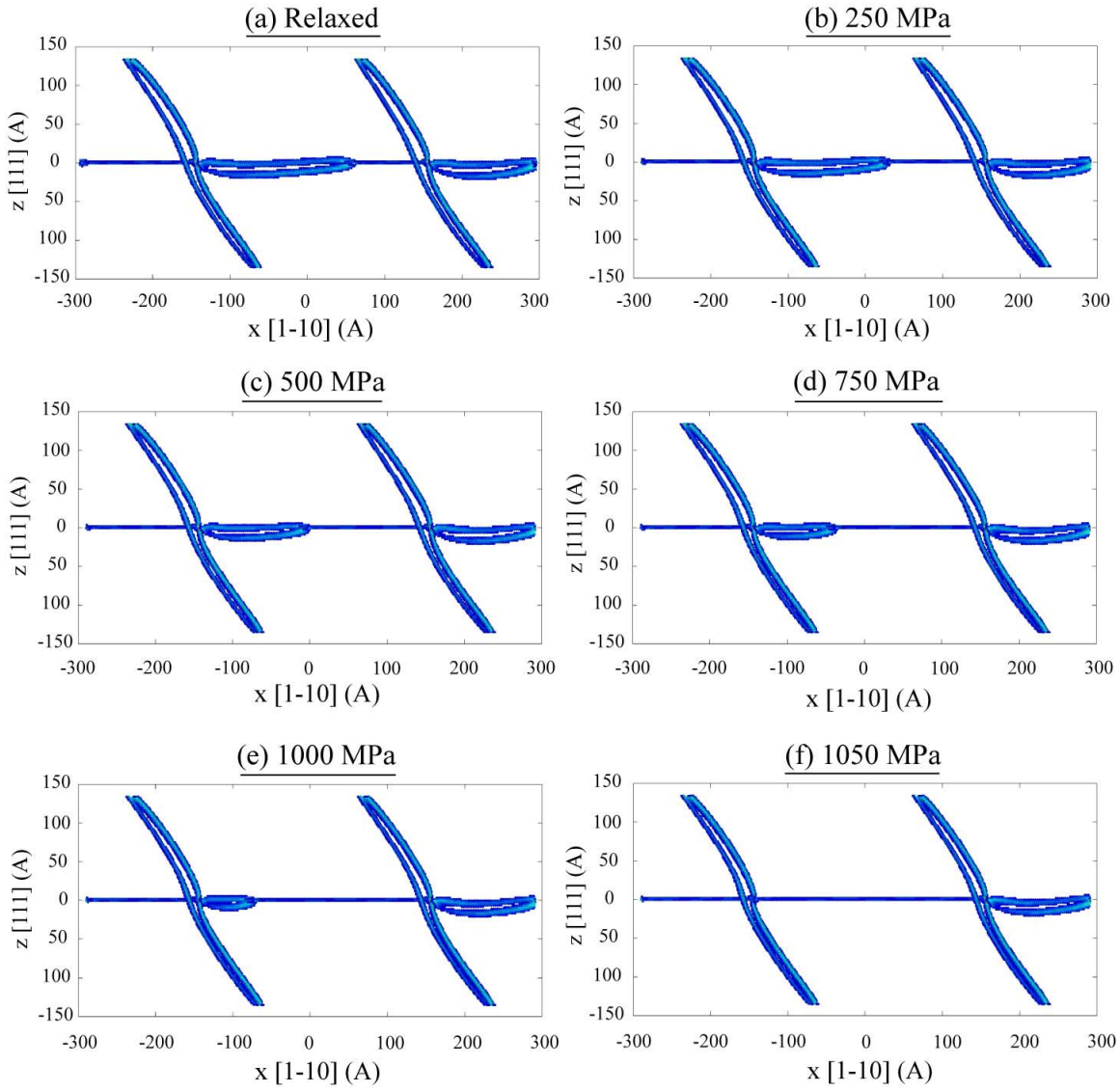
(a) Relaxed
(b) 250 MPa
(c) 500 MPa
(d) 750 MPa
(e) 1000 MPa
(f) 1050 MPa
z [111] (A)
x [1-10] (A)
150
100
50
0
50
100
-150
-300
-200
-100
0
100
200
300

Fig. 6:

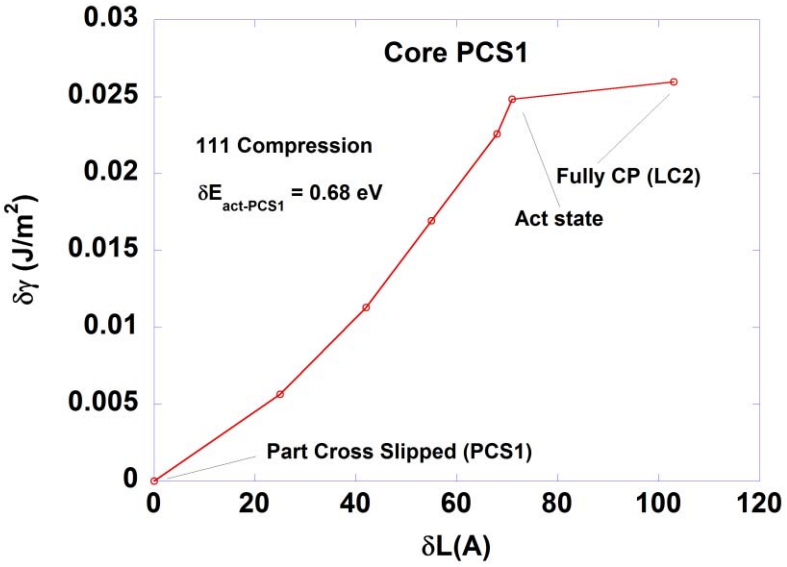
Core PCS1
111 Compression
$\delta E_{act-PCS1}$ = 0.68 eV
Fully CP (LC2)
Act state
Part Cross Slipped (PCS1)
$\delta\gamma$ (J/m^2)
δL(A)
0.03
0.025
0.02
0.015
0.01
0.005
0
0
20
40
60
80
100
120

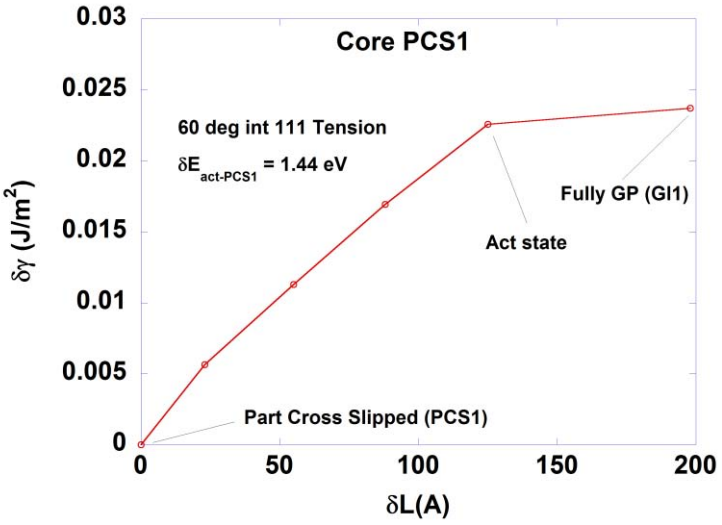
Core PCS1
60 deg int 111 Tension
$\delta E_{act-PCS1}$ = 1.44 eV
Fully GP (GI1)
Act state
Part Cross Slipped (PCS1)
$\delta\gamma$ (J/m^2)
δL(A)
0.03
0.025
0.02
0.015
0.01
0.005
0
0
50
100
150
200

Fig. 7:

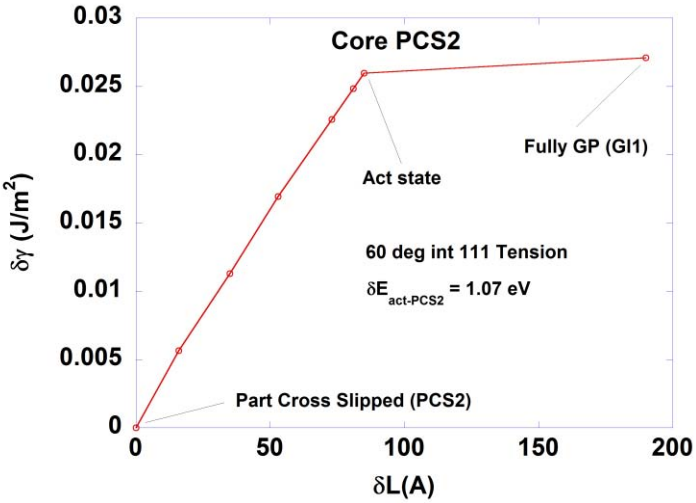
Core PCS2
Fully GP (Gl1)
Act state
60 deg int 111 Tension
δE act-PCS2 = 1.07 eV
Part Cross Slipped (PCS2)
δγ (J/m2)
δL(A)
0.03
0.025
0.02
0.015
0.01
0.005
0
0
50
100
150
200

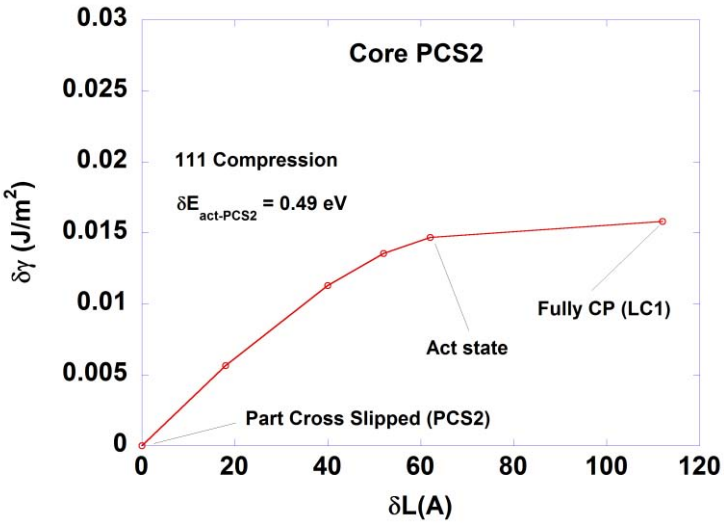
Core PCS2
111 Compression
δE act-PCS2 = 0.49 eV
Fully CP (LC1)
Act state
Part Cross Slipped (PCS2)
δγ (J/m2)
δL(A)
0.03
0.025
0.02
0.015
0.01
0.005
0
0
20
40
60
80
100
120

Fig. 8:

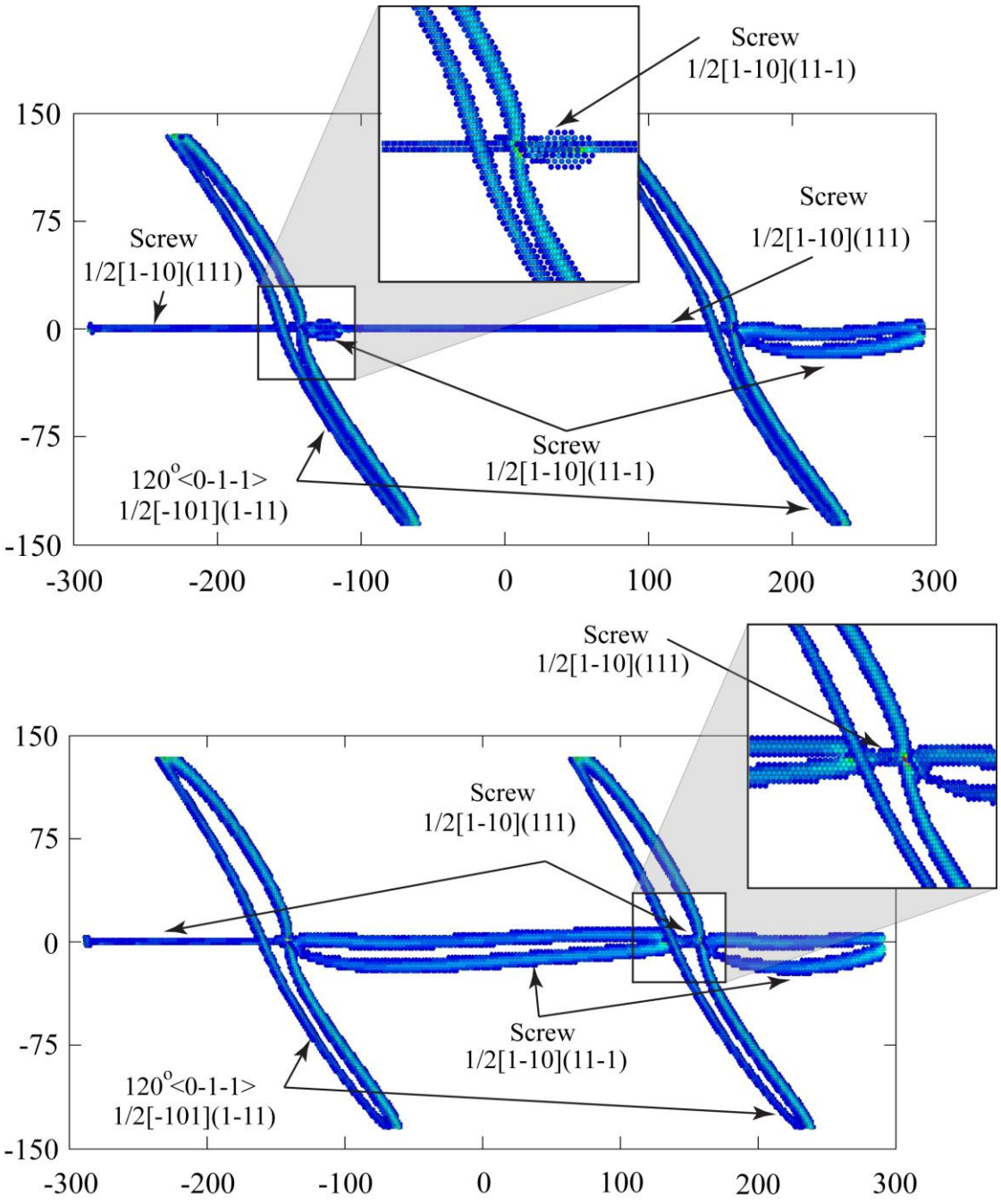
Screw
1/2[1-10](11-1)
Screw
1/2[1-10](111)
Screw
1/2[1-10](111)
Screw
1/2[1-10](11-1)
120°<0-1-1>
1/2[-101](1-11)
150
75
0
-75
-150
-300
-200
-100
0
100
200
300
Screw
1/2[1-10](111)
Screw
1/2[1-10](111)
Screw
1/2[1-10](11-1)
120°<0-1-1>
1/2[-101](1-11)
150
75
0
-75
-150
-300
-200
-100
0
100
200
300

Fig. 9:

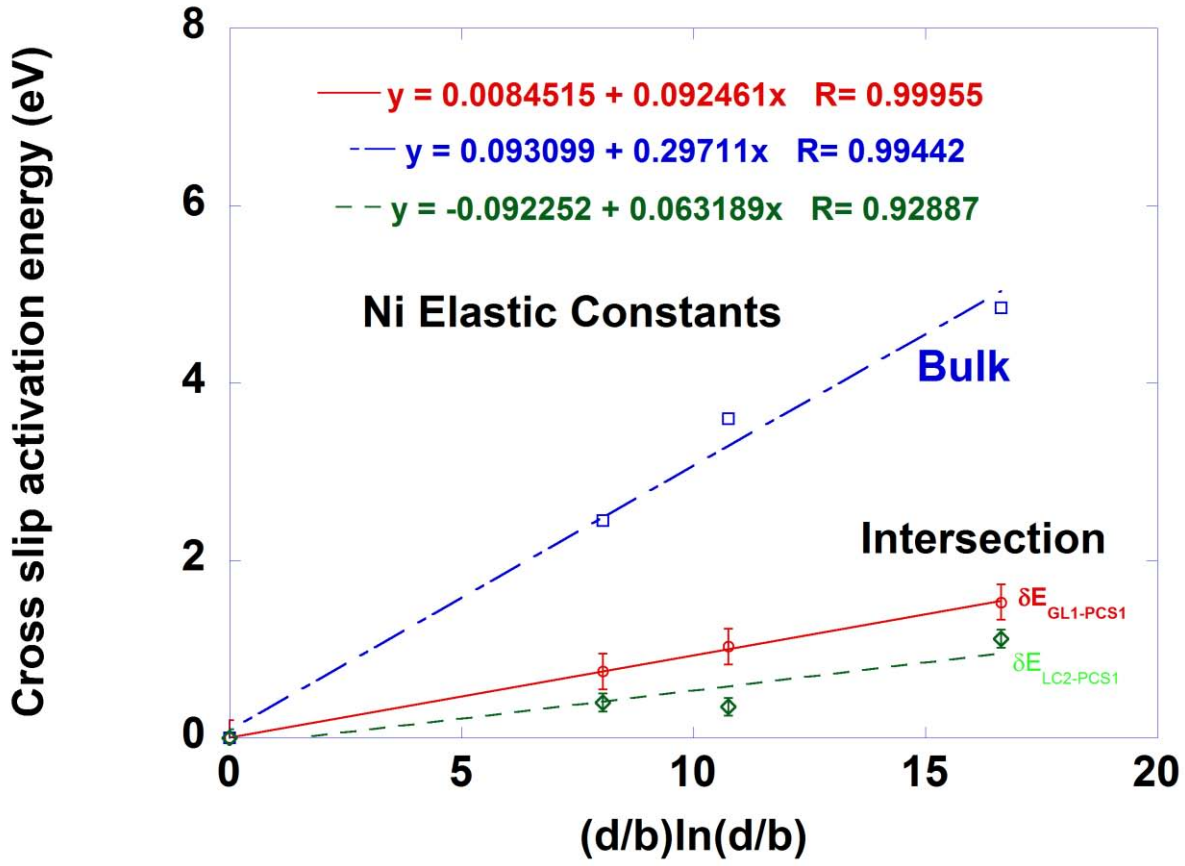
y = 0.0084515 + 0.092461x R= 0.99955
y = 0.093099 + 0.29711x R= 0.99442
y = -0.092252 + 0.063189x R= 0.92887
Ni Elastic Constants
Bulk
Intersection
δE GL1-PCS1
δE LC2-PCS1
Cross slip activation energy (eV)
(d/b)ln(d/b)
0
2
4
6
8
0
5
10
15
20

Fig. 10: